

Interplay among the azimuthally dependent HBT radii and the elliptic flow

Insights from the Buda-Lund hydro model

Máté Csanád¹, Boris Tomášik^{2,3}, and Tamás Csörgő⁴

¹ Eötvös University, H- 1117 Budapest XI, Pázmány Péter s. 1/A, Hungary

² Univerzita Mateja Bela, 97401 Banská Bystrica, Slovakia

³ FNSPE, Czech Technical University, Prague, Czech Republic

⁴ MTA KFKI RMKI, H-1525 Budapest 114, POBox 49, Hungary

November 3, 2018

Abstract. We present a calculation of the elliptic flow and azimuthal dependence of the correlation radii in the ellipsoidally symmetric generalization of the Buda-Lund model. The elliptic flow is shown to depend only on the flow anisotropy while in case of correlation radii both flow and space anisotropy play an important role in determining their azimuthal oscillation. We also outline a simple procedure for determining the parameters of the model from data.

PACS. 2 5.75.-q, 25.75.Gz, 25.75.Ld

1 Introduction

Studies of the freeze-out configuration in non-central ultra-relativistic nuclear collisions have yielded valuable information on the dynamics of the collision. The azimuthal asymmetry of hadronic momentum spectra—widely known under the somewhat vague term “elliptic flow”—is a cornerstone result for conclusions about thermalization and near perfect fluid dynamics [1]. The measurement of azimuthal dependence of correlation radii in non-central collisions indicates a fireball which breaks up while still being elongated out-of-reaction-plane [2]. This is the original orientation of the system and the observation thus provides an upper bound on the total lifespan of the created fireball and suggests an early and sudden freeze-out in a blast-wave picture, influentially suggested in ref. [3].

These observables can result from an interplay of spatial asymmetry of the fireball and the asymmetry of the flow velocity field of an exploding fireball. The question is if and how these asymmetries can be both determined from data. Such a question can be studied in the framework of a model. Here we present a study that utilizes the Buda-Lund hydro model.

For the present study we use the ellipsoidal Buda-Lund parametrization of the freeze-out of the fireball [4]. Note that the parameterization corresponds to a solution of certain class of hydrodynamic models [5,6,7,8].

We shall show that in the Buda-Lund model elliptic flow results solely from the flow asymmetry, and that the entanglement of spatial and flow anisotropy in determining the azimuthal oscillation of the correlation radii is

rather strong. This can be contrasted to other derivations that explore the conditions for quark coalescence [9], or the numerical solutions of boost-invariant, azimuthally dependent hydrodynamics with Gaussian initial conditions [10]. Azimuthally asymmetric HBT radii were also considered recently in cascade models, e.g. in the fast Monte-Carlo model of ref. [11], or, in the Hadronic Resonance Cascade [12]. A simple procedure to disentangle spatial and momentum space anisotropy from elliptic flow and azimuthally sensitive HBT measurements was proposed for generalized blast-wave type of models in ref. [13]. Now we investigate how to disentangle these effects in the ellipsoidally symmetric version of the Buda-Lund hydro model. Let us note that we cannot attempt to evaluate or fully cite all the relevant works in this technical paper, but we kindly refer the interested readers to the review of reviews in ref. [14], and also to ref. [15], a recent review that emphasizes the femtoscopy aspects of particle interferometry.

The structure of our paper is as follows: In Section 2 we shall shortly introduce the basic features of the ellipsoidally symmetric Buda-Lund model. Section 3 deals with the calculation of elliptic flow and Section 4 with determining the correlation radii. Finally, in Section 5 we present a simple strategy how various parameters of an azimuthally non-symmetric fireball can be obtained from data. We conclude in Section 6.

2 Buda-Lund model: basic features

Perfect fluid hydrodynamics is based on local conservation of entropy σ and four-momentum tensor $T^{\mu\nu}$,

$$\partial_\mu(\sigma u^\mu) = 0, \quad (1)$$

$$\partial_\nu T^{\mu\nu} = 0, \quad (2)$$

where u^μ stands for the four-velocity of the matter, which is normalized to unity as $u^\mu u_\mu = 1$. (Entropy conservation indicates that there are no dissipative terms like bulk or shear viscosity, and heat conduction, as any of these effects would lead to entropy production). For perfect fluids, the four-momentum tensor is diagonal in the local rest frame,

$$T^{\mu\nu} = (e + p)u^\mu u^\nu - pg^{\mu\nu}. \quad (3)$$

Here e stands for the local energy density and p for the pressure. The local conservation of energy, momentum and entropy yield five constraints on six unknowns (the three independent components of the four-velocity field and the three thermodynamical variables, the energy density, the entropy density and the pressure). These equations are closed by the equation(s) of state, which gives the relationship between e , p (and σ), sometimes as a function of yet another variables, like the temperature T .

We focus here on the analytic approach in exploring the consequences of the presence of such perfect fluids in high energy heavy ion experiments in Au+Au collisions at RHIC. Such exact analytic solutions were published recently in refs. [5,6,7,8,16]. In some of the recently found exact analytic solutions of relativistic hydrodynamics, the equation of state has a relatively simple form, typically $e - B = \kappa(p + B)$ is assumed, where B is a constant, called the bag constant which has a non-zero value in a quark-gluon plasma and has a vanishing value in the hadron gas phase. The parameter κ is either a constant like in ref. [16] or more generally, analytic solutions can be obtained even if $\kappa = \kappa(T)$ is an arbitrary, temperature dependent function, see for example the non-relativistic exact solutions in ref. [5].

A tool, that includes these above listed exact, dynamical hydro solutions, as well as some other cases, and interpolates among them, is the Buda-Lund hydro model of refs. [17,18]. This hydro model is successful in describing experimental data on single particle spectra and two-particle correlations [4,19].

The Buda-Lund hydro model [17] successfully describes BRAHMS, PHENIX, PHOBOS and STAR data on identified single particle spectra and the transverse mass dependent Bose-Einstein or HBT radii as well as the pseudorapidity distribution of charged particles in central Au + Au collisions both at $\sqrt{s_{NN}} = 130$ GeV [19] and at $\sqrt{s_{NN}} = 200$ GeV [4] and in p+p collisions at $\sqrt{s} = 200$ GeV [20], as well as data from Pb+Pb collisions at CERN SPS [21] and $h + p$ reactions at CERN SPS [22,23]. The model is defined with the help of its emission function; to take into account the effects of long-lived resonances, it utilizes the core-halo model [24].

In the Buda-Lund model, the emission function is given by that of a hydrodynamically expanding fireball, surrounded by a halo of long lived resonances. In this paper, we assume the validity of the core-halo model, i.e. that the long-lived resonances create an unresolved, narrow peak in the two-particle HBT correlation function, which results in an effective intercept parameter λ . The integrals of the emission function of the hydrodynamically expanding core are evaluated [22] in a saddle-point approximation. When an improved saddle-point calculation is performed, effective binary sources and related non-Gaussian behavior is seen in this model, in particular in the longitudinal direction [22]. However, in a Gaussian approximation, using a single saddle point in the integration, the effective Buda-Lund emission function looks like:

$$S(x, k) d^4x = \frac{g}{(2\pi)^3} \frac{p^\mu u_\mu(x_f) H(\tau_f)}{B(x_f, p) + s_q} \times \exp[-R_{\mu\nu}^{-2}(x - x_f)^\mu(x - x_f)^\nu] d^4x, \quad (4)$$

where g is the degeneracy factor ($g = 1$ for identified pseudoscalar mesons, $g = 2$ for identified spin=1/2 baryons), $B(x, p)$ is the (inverse) Boltzmann phase-space distribution, the term s_q is determined by quantum statistics, $s_q = 0, -1$, and $+1$ for Boltzmann, Bose-Einstein and Fermi-Dirac distributions, respectively, and the space-time four-vector of the point of maximal emissivity (or freeze-out) $x_f \equiv x_f(p)$ depends on the momentum of the emitted particles. The time dependence of the emission is described by $H(\tau)$, and

$$R_{\mu\nu}^{-2} = \partial_\mu \partial_\nu (-\ln(S_0))(x_f, p), \quad (5)$$

is the 'width' of the emission function, introducing S_0 , as the 'main' part of the emission function:

$$S_0(x, p) = \frac{H(\tau)}{B(x, p) + s_q}. \quad (6)$$

For a relativistic, hydrodynamically expanding system, the (inverse) Boltzmann phase-space distribution is

$$B(x, p) = \exp\left(\frac{p \cdot u(x)}{T(x)} - \frac{\mu(x)}{T(x)}\right). \quad (7)$$

We will utilize some ansatz for the shape of the flow four-velocity, $u_\nu(x)$, chemical potential, $\mu(x)$, and temperature, $T(x)$ distributions. Their form is determined with the help of exact solutions of hydrodynamics, both in the relativistic [6,16,8] and in the non-relativistic cases [25,26,27,28], with the conditions that these distributions are characterized by mean values and variances, and that they lead to (simple) analytic formulas when evaluating particle spectra and two-particle correlations.

The solution is scale-invariant with the following scaling variable:

$$s = \frac{r_x^2}{X^2} + \frac{r_y^2}{Y^2} + \frac{r_z^2}{Z^2}. \quad (8)$$

The velocity field is

$$u(x) = (\gamma, r_x \frac{\dot{X}}{X}, r_y \frac{\dot{Y}}{Y}, r_z \frac{\dot{Z}}{Z}), \quad (9)$$

with γ being the appropriate factor to ensure $u \cdot u = 1$.

For the fugacity distribution we assume a shape, that leads to Gaussian profile in the non-relativistic limit,

$$\frac{\mu(x)}{T(x)} = \frac{\mu_0}{T_0} - s, \quad (10)$$

corresponding to the solution discussed in refs. [25,26,5]. We assume that the temperature may depend on the position as well as on proper-time. We characterize the inverse temperature distribution similarly to the shape used in the axially symmetric model of ref. [17,29], and discussed in the exact hydro solutions of refs [25,26],

$$\frac{1}{T(x)} = \frac{1}{T_0} \left(1 + \frac{T_0 - T_s}{T_s} s \right) \left(1 + \frac{T_0 - T_e}{T_e} \frac{(\tau - \tau_0)^2}{2\Delta\tau^2} \right), \quad (11)$$

where T_0 and T_s are the temperatures of the center, and the surface at the mean freeze-out time τ_0 , while T_e corresponds to the temperature of the center after most of the particle emission is over (cooling due to evaporation and expansion). Sudden emission corresponds to $T_e = T_0$, and the $\Delta\tau \rightarrow 0$ limit. It is convenient to introduce the following quantities

$$a^2 = \frac{T_0 - T_s}{T_s} = \left\langle \frac{\Delta T}{T} \right\rangle_{\perp}, \quad (12)$$

$$d^2 = \frac{T_0 - T_e}{T_e} = \left\langle \frac{\Delta T}{T} \right\rangle_{\tau} \quad (13)$$

The time dependence of the emission, described by $H(\tau)$ can be approximated with a Gaussian representation of the Dirac-delta distribution around the freeze-out proper-time τ_f ,

$$H(\tau) = \frac{1}{(2\pi\Delta\tau^2)^{1/2}} \exp\left(-\frac{(\tau - \tau_f)^2}{2\Delta\tau^2}\right), \quad (14)$$

with $\Delta\tau$ being the proper-time duration of the particle production.

From now on our investigations will be performed at *midrapidity*. With the above shorthands, at midrapidity the Boltzmann factor at the freeze-out will have the following form:

$$B(x_f, p) = \exp\left(\frac{p_x^2}{2m_t T_x} + \frac{p_y^2}{2m_t T_y} - \frac{p_t^2}{2m_t T_0} + \frac{m_t}{T_0} - \frac{\mu_0}{T_0}\right), \quad (15)$$

where $m_t = \sqrt{p_t^2 + m^2}$ and the direction dependent slope parameters are

$$T_x = T_0 + m_t \dot{X}^2 \frac{T_0}{T_0 + m_t a^2}, \quad (16)$$

$$T_y = T_0 + m_t \dot{Y}^2 \frac{T_0}{T_0 + m_t a^2}. \quad (17)$$

3 Elliptic flow

The result for the elliptic flow, that comes directly from a perfect hydro solution is the following simple scaling

law [5,18]

$$v_2 = \frac{I_1(w)}{I_0(w)}, \quad (18)$$

where $I_n(z)$ stands for the modified Bessel function of the second kind, $I_n(z) = (1/\pi) \int_0^\pi \exp(z \cos(\theta)) \cos(n\theta) d\theta$. The scaling variable

$$w = \frac{p_t^2}{4m_t} \left(\frac{1}{T_y} - \frac{1}{T_x} \right). \quad (19)$$

This can also be written as

$$w = E_K \frac{\epsilon}{T_{\text{eff}}}, \quad (20)$$

where E_K is a relativistic generalization of the transverse kinetic energy, defined as

$$E_K = \frac{p_t^2}{2m_t}, \quad (21)$$

and we have introduced T_{eff} , the effective slope of the azimuthally averaged single particle p_t spectra as the harmonic mean of the slope parameters in the in-plane and in the out-of-plane transverse directions,

$$T_{\text{eff}} = 2 \left(\frac{1}{T_x} + \frac{1}{T_y} \right)^{-1}, \quad (22)$$

and momentum space eccentricity parameter

$$\epsilon = \frac{T_x - T_y}{T_x + T_y}. \quad (23)$$

If there is no transverse temperature gradient ($a = 0$), then this simplifies as

$$\epsilon = \frac{\dot{X}^2 - \dot{Y}^2}{\dot{X}^2 + \dot{Y}^2 + 2T_0/m_t}, \quad (24)$$

(see refs. [5,18,30] for details).

Thus the Buda-Lund hydro model predicted [5,18] a *universal scaling* of the elliptic flow: every v_2 measurement is predicted to fall on the same scaling curve I_1/I_0 when plotted against the scaling variable w . This means, that v_2 depends on any physical parameter (transverse or longitudinal momentum, mass, center of mass energy, collision centrality, type of the colliding nucleus etc.) only through w .

We note, that for a leading order approximation, $E_K \approx m_t - m$, which also explains recent development on scaling properties of v_2 by the PHENIX experiment at midrapidity [31,32].

In general, the azimuthal anisotropy of hadronic momentum spectrum is generated by the azimuthal variation of both the absolute magnitude of the expansion velocity and its orientation. The same elliptic flow parameter v_2 can be obtained by different combinations of these two and it has been shown in the framework of blast-wave model that by modifying the latter one can completely

change (even invert) the dependence of v_2 on the former [33]. Technically, this shows up as a dependence of the elliptic flow on both the spatial anisotropy and the flow anisotropy.

We see from eqs. (18)–(24) that in Buda-Lund model the velocity field is oriented in such a way that the spatial anisotropy of the hadronic freeze-out stage plays no role in determining v_2 : eq. (18) depends only on the transverse expansion rates \dot{X} and \dot{Y} , but it does not depend on the actual source sizes X and Y . Only difference of the slope parameters T_x and T_y is important for the elliptic flow. Thus the elliptic flow vanishes in this model, if $\dot{X} = \dot{Y}$, indicating that if the expansion rates are similar in the in-plane and out-of-plane transverse directions, $v_2 = 0$. In this sense, we may write that v_2 in the Buda-Lund model is driven by the difference of the in-plane and out-of-plane transverse expansion rates of the fluid, during the hadronic final state.

In order to compare more easily the Buda-Lund model results for the elliptic flow with the azimuthally sensitive extension of the blast-wave model [2,33], we introduce ρ_0 and ρ_2 so that

$$\dot{X} = \rho_0(1 + \rho_2) \quad (25a)$$

$$\dot{Y} = \rho_0(1 - \rho_2) \quad (25b)$$

therefore

$$\rho_0 = \frac{1}{2} (\dot{X} + \dot{Y}) \quad (26a)$$

$$\rho_2 = \frac{\dot{X} - \dot{Y}}{\dot{X} + \dot{Y}}. \quad (26b)$$

The elliptic flow in the Buda-Lund model also depends on the transverse temperature gradient a of eq. (12). It actually moderates the difference between T_x and T_y and increases the elliptic flow at given ρ_2 . The dependence of v_2 on flow anisotropy ρ_2 and temperature gradient a is shown in Fig. 1.

4 Azimuthally dependent correlation radii

The two-particle Bose-Einstein correlation function from the Buda-Lund source function (defined in eq. (4)) is most naturally calculated in the frame given by the main axes of the ellipsoid. The result is

$$C(q) = 1 + \lambda e^{-q_0^2 \Delta\tau_*^2 - q_x^2 R_{*,x}^2 - q_y^2 R_{*,y}^2 - q_z^2 R_{*,z}^2} \quad (27)$$

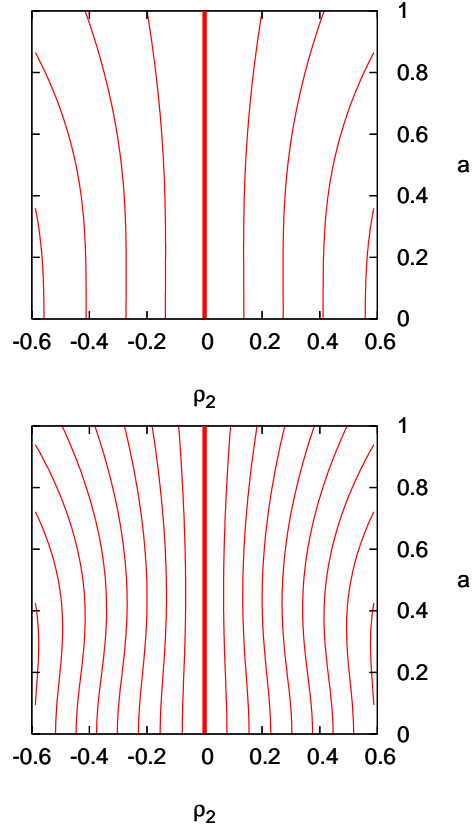


Fig. 1. Lines of constant v_2 of pions as function of ρ_2 and a . The increment between neighboring contours is 0.05, the thick curve shows $v_2 = 0$. The sign of v_2 is the same as the sign of ρ_2 . Transverse momentum is 0.5 GeV/c (top) and 1 GeV/c (bottom). Other parameters in the calculation were motivated by data (see Section 5): $T_0 = 163$ MeV, $\rho_0 = 0.61$.

with λ being the intercept parameter, $q = p_1 - p_2$, and

$$\frac{1}{\Delta\tau_*^2} = \frac{1}{\Delta\tau^2} + \frac{m_t d^2}{T_0 \tau_0^2}, \quad (28a)$$

$$R_{*,x}^2 = X^2 \left(1 + \frac{m_t (a^2 + \dot{X}^2)}{T_0} \right)^{-1}, \quad (28b)$$

$$R_{*,y}^2 = Y^2 \left(1 + \frac{m_t (a^2 + \dot{Y}^2)}{T_0} \right)^{-1}, \quad (28c)$$

$$R_{*,z}^2 = Z^2 \left(1 + \frac{m_t (a^2 + \dot{Z}^2)}{T_0} \right)^{-1}. \quad (28d)$$

Note that parameter d makes the effective life-time and the difference between the out and the side radius components momentum dependent.

From the mass-shell constraint of $p_1^2 = p_2^2 = m^2$ one finds that

$$q_0 = \beta_x q_x + \beta_y q_y + \beta_z q_z \quad (29)$$

where $\beta = \mathbf{K}/K^0 = (\mathbf{p}_1 - \mathbf{p}_2)/(p_1^0 - p_2^0)$. Thus we can rewrite eq. (27) to

$$C(q) = 1 + \lambda \exp \left(- \sum_{i,j=x,y,z} R_{ij}^2 q_i q_j \right) \quad (30)$$

with the modified radii of

$$R_x^2 = R_{*,x}^2 + \beta_x^2 \Delta\tau_*^2, \quad (31a)$$

$$R_y^2 = R_{*,y}^2 + \beta_y^2 \Delta\tau_*^2, \quad (31b)$$

$$R_z^2 = R_{*,z}^2 + \beta_z^2 \Delta\tau_*^2, \quad (31c)$$

$$R_{xz}^2 = \beta_x \beta_z \Delta\tau_*^2, \quad (31d)$$

$$R_{yz}^2 = \beta_y \beta_z \Delta\tau_*^2, \quad (31e)$$

$$R_{xy}^2 = \beta_x \beta_y \Delta\tau_*^2. \quad (31f)$$

The above formulas are given in the frame, specified by the main axes of the expanding, ellipsoidally symmetric fireball. In general, this frame is rotated [5] with respect to the standard out-side-long system [34], which is given by the beam direction (longitudinal) and the transverse component of the pair momentum (outward). The correlation function in this out-side-long system is parameterized as

$$C(q) = 1 + \lambda e^{-q_o^2 R_o^2 - q_s^2 R_s^2 - q_l^2 R_l^2 - 2(q_o q_s R_{os} + q_o q_l R_{ol} + q_s q_l R_{sl})}. \quad (32)$$

We denote by ϑ the tilt angle between the longitudinal direction and the z -axis and φ stands for the angle between the outward direction and the plane given by x and z axes—the reaction plane. In the new frame we obtain azimuthally sensitive HBT radii that are given as

$$R_o^2 = R_x'^2 \cos^2 \varphi + R_y'^2 \sin^2 \varphi + R_{xy}'^2 \sin(2\varphi), \quad (33a)$$

$$R_s^2 = R_x'^2 \sin^2 \varphi + R_y'^2 \cos^2 \varphi - R_{xy}'^2 \sin(2\varphi), \quad (33b)$$

$$R_l^2 = R_x'^2 \sin^2 \vartheta + R_z'^2 \cos^2 \vartheta + R_{xz}'^2 \sin(2\vartheta), \quad (33c)$$

$$2R_{os}^2 = -R_x'^2 \sin(2\varphi) + R_y'^2 \sin(2\varphi) + 2R_{xy}'^2 \cos(2\varphi), \quad (33d)$$

$$2R_{sl}^2 = (R_x'^2 \sin(2\vartheta) + R_z'^2 \sin(2\vartheta) - 2R_{xz}'^2 \cos(2\vartheta)) \sin \varphi + (2R_{xy}'^2 \sin \vartheta + 2R_{yz}'^2 \cos \vartheta) \cos \varphi, \quad (33e)$$

$$2R_{lo}^2 = (R_x'^2 \sin(2\vartheta) - R_z'^2 \sin(2\vartheta) + 2R_{xz}'^2 \cos(2\vartheta)) \cos \varphi + (2R_{xy}'^2 \sin \vartheta + 2R_{yz}'^2 \cos \vartheta) \sin \varphi, \quad (33f)$$

where we have introduced

$$R_x'^2 = R_x^2 \cos^2 \vartheta + R_z^2 \sin^2 \vartheta - R_{xz}^2 \sin(2\vartheta) \quad (34)$$

$$R_{xy}'^2 = R_{xy}^2 \cos \vartheta - R_{yz}^2 \sin \vartheta \quad (35)$$

If the fireball is not tilted in the reaction plane ($\vartheta = 0$), which might appear at very high collision energies, then in the longitudinally co-moving frame (LCMS, $\beta_l = 0$) the

formulas further simplify as

$$R_o^2 = R_{*,x}^2 \cos^2 \varphi + R_{*,y}^2 \sin^2 \varphi + \beta_o^2 \Delta\tau_*^2 \quad (36a)$$

$$= \frac{R_{*,x}^2 + R_{*,y}^2}{2} + \beta_o^2 \Delta\tau_*^2 - \frac{R_{*,y}^2 - R_{*,x}^2}{2} \cos(2\varphi)$$

$$R_s^2 = R_{*,x}^2 \sin^2 \varphi + R_{*,y}^2 \cos^2 \varphi \quad (36b)$$

$$= \frac{R_{*,x}^2 + R_{*,y}^2}{2} + \frac{R_{*,y}^2 - R_{*,x}^2}{2} \cos(2\varphi),$$

$$R_{os}^2 = \frac{R_{*,y}^2 - R_{*,x}^2}{2} \sin(2\varphi), \quad (36c)$$

$$R_l^2 = R_{*,z}^2, \quad (36d)$$

$$R_{ol}^2 = 0, \quad (36e)$$

$$R_{sl}^2 = 0. \quad (36f)$$

It is convenient to decompose the correlation radii into Fourier series in azimuthal angle [35, 36]. Here, it is particularly trivial since there are only zeroth and second order terms

$$R_o^2 = R_{o,0}^2 + R_{o,2}^2 \cos(2\varphi) \quad (37a)$$

$$R_s^2 = R_{s,0}^2 + R_{s,2}^2 \cos(2\varphi) \quad (37b)$$

$$R_l^2 = R_{l,0}^2 \quad (37c)$$

$$R_{os}^2 = R_{os,0}^2 + R_{os,2}^2 \sin(2\varphi). \quad (37d)$$

In this Gaussian single saddle point version of the Buda-Lund model there is no implicit azimuthal dependence of the homogeneity regions. Thus the complete dependence on φ is written in eqs. (36). In such a case we observe rather known features:

- The oscillation amplitudes $|R_{o,2}^2|$, $|R_{s,2}^2|$, and $|R_{os,2}^2|$ are equal.
- The effective duration of particle emission can be obtained from the difference of non-oscillating parts as

$$\beta_o^2 \Delta\tau_*^2 = R_{o,0}^2 - R_{s,0}^2; \quad (38)$$

- We can extract the effective source sizes $R_{*,x}^2$ and $R_{*,y}^2$ from data as

$$R_{*,x}^2 = R_{s,0}^2 - R_{s,2}^2, \quad (39a)$$

$$R_{*,y}^2 = R_{s,0}^2 + R_{s,2}^2. \quad (39b)$$

If the first feature is not observed, or, if data lead to a negative r.h.s. of eq. (38), this would indicate that the above presented Gaussian version of the Buda-Lund model is not applicable for the description of that given data. It is however well known, already in the first formulation of the Buda-Lund model, ref. [17], the r.h.s. of eq. (38) can be negative. The exact hydro solutions and symmetry arguments require that $R_{s,0} = R_{o,0}$ in the vanishing transverse momentum limit only, otherwise at finite transverse momentum, $R_{s,0} > R_{o,0}$ is allowed in general. Such a behavior happens in exact, ring of fire type of hydrodynamical solutions, which were found in fireball hydrodynamics in ref. [26]. Such rings of fire type of exact hydro solutions appear if the radial flow is moderate and the temperature

distribution is very inhomogeneous, in our present notation if $a^2 \gg m\rho_0^2/(2T_0)$, while nearly Gaussian fireballs appear, if the temperature is nearly homogeneous and the radial flow is strong, $a^2 \ll m\rho_0^2/(2T_0)$. The data discussed in the present paper correspond to this latter limit.

So if there is a significant negative value for $R_{o,0}^2 - R_{s,0}^2$ in some data set, the shell of fire type of Buda-Lund solutions can be utilized, as a generalization of the present approach. as e.g. discussed also in refs. [22, 25]. Such shell of fire structures are also seen in blastwave models, see e.g. Figs. 18 and 19 of ref. [2] and also in cascade calculations e.g. in Fig. 12 of ref.[12].

The azimuthal dependence of correlation radii may be due to spatial deformation of the fireball as well as due to azimuthal dependence of the expansion velocity field. The interplay of these two effects in framework of the blast-wave model has been studied in [33]. In order to compare with that paper we parameterize the transverse scales with the help of average radius R and asymmetry parameter a_s

$$X = a_s R \quad Y = \frac{R}{a_s}, \quad (40)$$

(note that a_s corresponds to a of [33]).

The amplitude of oscillation trivially scales with the absolute size of the fireball. We want to scale out this effect in order to directly see the effect of eccentricity. Thus we shall be interested in *scaled* oscillation amplitudes $R_{s,2}^2/R_{s,0}^2$. (For the outward radius the result would be similar—scaled amplitude would be just slightly smaller due to added $\beta_o^2 \Delta\tau_*^2$ term in the denominator.) Such a ratio then does not depend on R and from eqs.(28), (36c), and (40) we derive

$$\frac{R_{s,2}^2}{R_{s,0}^2} = \frac{\frac{a_s^{-2}}{1+m_t T_0^{-1} (a^2 + \rho_0^2 (1-\rho_2)^2)} - \frac{a_s^2}{1+m_t T_0^{-1} (a^2 + \rho_0^2 (1+\rho_2)^2)}}{\frac{a_s^{-2}}{1+m_t T_0^{-1} (a^2 + \rho_0^2 (1-\rho_2)^2)} + \frac{a_s^2}{1+m_t T_0^{-1} (a^2 + \rho_0^2 (1+\rho_2)^2)}} \quad (41)$$

We plot these scaled oscillation amplitudes in Figure 2 as functions of a_s and ρ_2 . The correlation between spatial and flow asymmetry is well pronounced: one can get the same oscillation with different pairs of values for the two parameters. Note that the dependence on flow anisotropy ρ_2 in the Buda-Lund model is much stronger than in the blast-wave model of refs. [2] and [33] (Model 1 of the latter paper).

There is an additional parameter in the Buda-Lund model, which influences the oscillation: the transverse temperature gradient a defined in eq. (12). We plot the dependence of scaled oscillation amplitude on a and a_s in Figure 3. From eq. (41) one can infer that the amplitude does not depend of a if $\rho_2 = 0$. For the plots we have chosen $\rho_2 = 0.3$. Increasing a tends to wash away the dependence of the amplitude on ρ_2 , as seen from eq. (41).

5 Strategy of analysis

In this section we outline how one can infer the model parameters from data on (i) azimuthally integrated spectra,

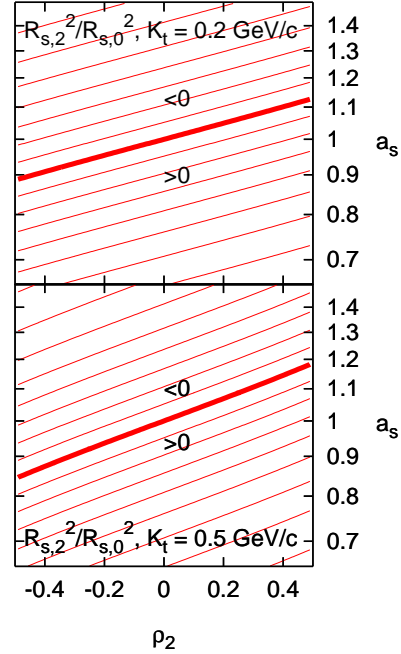


Fig. 2. Curves of constant $R_{s,2}^2/R_{s,0}^2$ calculated as functions of a_s and ρ_2 at fixed $a = 0$. Temperature $T_0 = 163$ MeV and $\rho_0 = 0.61$ (as obtained in Section 5). Increments between the contours are 0.1, thick lines show $R_{s,2}^2/R_{s,0}^2 = 0$. Pair momentum K_t was chosen 0.2 GeV (upper panel) and 0.5 GeV (lower panel).

(ii) elliptic flow, (iii) azimuthally and transverse momentum dependent correlation radii.

For a simple analysis strategy, one might observe, that approximate formulas can be derived assuming that the flow anisotropy parameter is small, $\rho_2 \ll 1$. Keeping the leading order terms in this expansion, the following approximative formulas are obtained:

$$T_{\text{eff}} = T_0 + M\rho_0^2 + \mathcal{O}(\rho_2^2), \quad (42)$$

$$M = m_t \frac{T_0}{T_0 + m_t a^2}, \quad (43)$$

$$v_2 \simeq \frac{p_t^2}{2m_t M} \frac{\rho_2}{\rho_0^2} \frac{1}{\left(1 + \frac{T_0}{M\rho_0^2}\right)^2}. \quad (44)$$

Here, T_{eff} is the effective slope parameter of *azimuthally integrated* $m_t - m$ spectrum. Let us observe, that this effective temperature depends on the freeze-out temperature scale T_0 and on the radial flow coefficient ρ_0 , but to a leading order, it does not depend on the flow anisotropy parameter ρ_2 . In contrast, the elliptic flow is increasing linearly with ρ_2 . Thus, naively, one expects that the mass dependence of the slope parameters can be utilized to determine the freeze-out temperature T_0 and the radial flow parameter ρ_0 , then using these parameters one could extract the flow anisotropy parameter ρ_2 from the data on the elliptic flow v_2 .

If the temperature inhomogeneity parameter is very small, $a^2 \ll T_0/m_t$, then $M \approx m_t$, and one can adopt

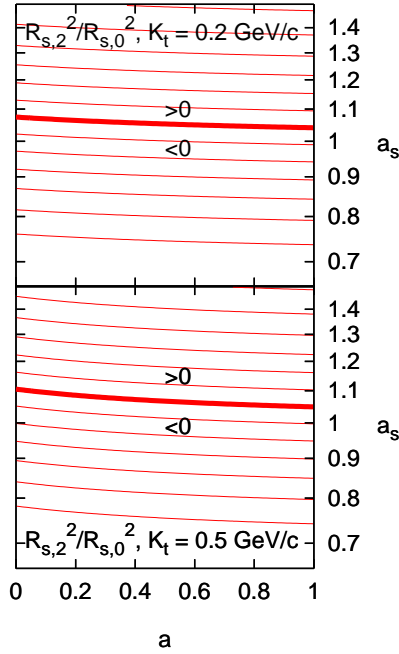


Fig. 3. Curves of constant $R_{s,2}^2/R_{s,0}^2$ calculated as functions of a_s and a at fixed $\rho_0 = 0.3$. Temperature $T_0 = 163$ MeV and $\rho_0 = 0.61$ (as obtained in Section 5). Increments between the contours are 0.1, thick lines show $R_{s,2}^2/R_{s,0}^2 = 0$. Pair momentum K_t was chosen 0.2 GeV (upper panel) and 0.5 GeV (lower panel).

such a simple minded strategy. Let us then consider the HBT radii in this $a \simeq 0$ case:

$$R_s \simeq \frac{R_{*,x}^2 + R_{*,y}^2}{2} + \frac{R_{*,y}^2 - R_{*,x}^2}{2} \cos 2\varphi \quad (45)$$

$$R_{*,x} \simeq X^2 \frac{T_0}{T_0 + m_t \dot{X}^2}, \quad (46)$$

$$R_{*,y} \simeq Y^2 \frac{T_0}{T_0 + m_t \dot{Y}^2}. \quad (47)$$

As \dot{X} and \dot{Y} are given by ρ_0 and ρ_2 the new fit parameters will be the actual sizes X and Y . So if $a = 0$, one can obtain the freeze-out temperature and the radial flow parameter from the mass dependence of the slopes, then momentum anisotropy parameter ρ_2 can be obtained from v_2 using T_0 and ρ_0 , finally X and Y come from the HBT radii. However, the temperature inhomogeneity parameter a^2 couples to all expressions through the effective mass scale M defined above, and makes such a simple strategy impractical, except in the case of $a = 0$.

As such a naive strategy cannot be applied in the general case, because parameter a appears in a non-trivial manner in both the slope, the elliptic flow and the HBT data, we have tried to do a simultaneous description of slope parameters, elliptic flow and HBT radii. To estimate a reasonable range of the model parameters, we first have selected a centrality class, 20-30%, where such data are available.

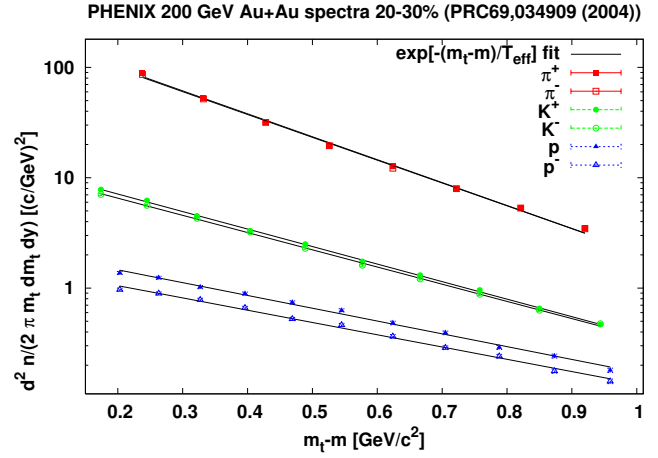


Fig. 4. The exponential fits to PHENIX identified pion, kaon, proton (and antiparticle) spectra from 20-30% centrality class.

Particle:	m (MeV)	T_{eff} (MeV)
π^+	139	210.2 ± 0.8
K^+	494	284.4 ± 2.2
p	938	414.8 ± 7.5
π^-	139	211.9 ± 0.7
K^-	494	278.1 ± 2.2
\bar{p}	938	434.7 ± 8.6

Table 1. Exponential slope parameters extracted from PHENIX weak decay corrected identified particle spectra in 20-30 % most central Au+Au collisions at $\sqrt{s_{NN}} = 200$ GeV. Errors are statistical only.

First, we have obtained the slopes of single-particle azimuthally integrated spectra in $m_t - m$. The exponential fits to PHENIX identified pion, kaon, proton (and antiparticle) spectra from 20-30% centrality class are obtained in just the same way as it was done for other centrality classes in ref. [37]: $\frac{d^2 n}{(2\pi m_t dm_t dy)}$ was fitted to $\frac{A}{2\pi T_{\text{eff}}(T_{\text{eff}} + m)} \exp(-\frac{m_t - m}{T_{\text{eff}}})$. The fit range was $0.2 \text{ GeV} < m_t - m < 1 \text{ GeV}$ for π^+ and π^- , while it was $0.1 \text{ GeV} < m_t - m < 1 \text{ GeV}$ for K^+ , K^- , p and \bar{p} . The fits are shown in Figure 4 and effective temperatures are summarized in Table 1. PHENIX spectra were used here because they are corrected for weak decays.

In the second step we describe qualitatively the RHIC 20-30% central $\sqrt{s_{NN}} = 200 \text{ GeV}$ Au+Au data. We compared the full Buda-Lund formulas for the slopes, elliptic flow and azimuthally sensitive HBT radii, eqs. (18), (19), (22), (28b), and (28c) to azimuthally sensitive HBT radii from STAR [39], the mass dependence of effective temperatures from PHENIX [37], and pion v_2 data from STAR [38]. For such an overall procedure, the fit parameters are T_0 , X , Y , ρ_0 , ρ_2 and a . One can get $R_{*,x}$ and $R_{*,y}$ via eqs. (39). The Buda-Lund calculations are compared with data in Fig. 5 for the following parameter values: $T_0 = 163$ MeV, $\rho_0 = 0.61$, $\rho_2 = 0.17$, $X^2 = 33.5 \text{ fm}^2$,

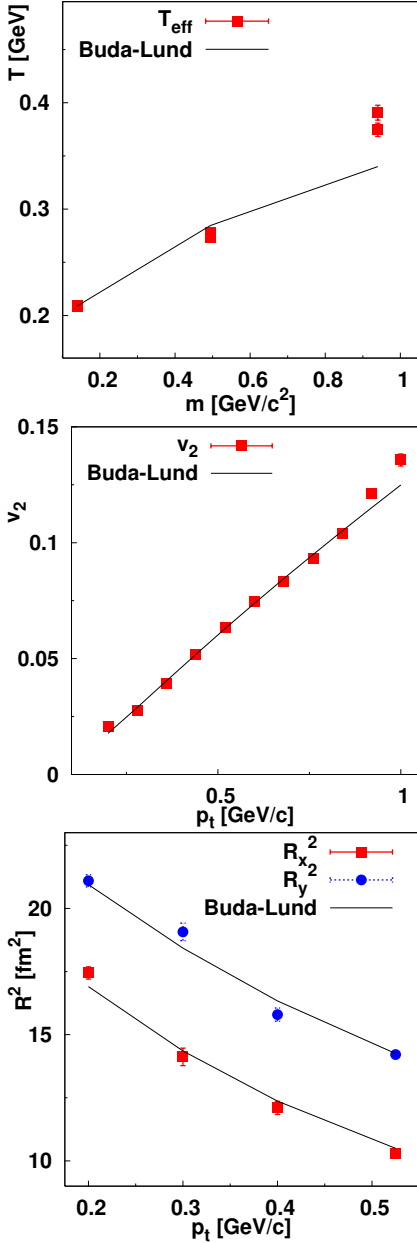


Fig. 5. The top panel shows the Buda-Lund calculations compared to slope parameters obtained from PHENIX weak decay corrected invariant momentum distribution data [37] in the 20-30% centrality class. The middle panel shows a comparison to pion v_2 data from STAR [38] in the same centrality class. The bottom panel shows the Buda-Lund comparison to azimuthally sensitive HBT radii from STAR [39], also measured in 20-30% central $\sqrt{s_{NN}} = 200$ GeV Au+Au collisions. We used the full Buda-Lund formulas for the slopes, elliptic flow and azimuthally sensitive HBT radii, eqs. (18), (19), (22), (28b), and (28c), and the same parameter values of $T_0 = 163$ MeV, $\rho_0 = 0.61$, $\rho_2 = 0.17$, $X^2 = 33.5$ fm², $Y^2 = 33.9$ fm², and $a^2 = 0.16$ were used in all the three panels.

$Y^2 = 33.9$ fm² and $a^2 = 0.16$. These results indicate that the theoretical formulas developed in the present paper are reasonable and could be utilized to describe qualitatively the azimuthally sensitive data at in $\sqrt{s_{NN}} = 200$ GeV Au+Au collisions at RHIC.

6 Conclusions

We have shown that in the Buda-Lund model the expansion of the velocity field is oriented in such a way that the elliptic flow only depends on the asymmetry of the expansion velocity in the directions in and out of the reaction plane. Unlike the blast-wave model, there is no influence of the elliptic shape of transverse cross-section.

Oscillation of the transverse correlation radii is shaped by flow as well as spatial anisotropy. This is again different from the blast-wave model: in the azimuthally non-symmetric generalization of that model which was able to describe RHIC data, correlation radii mainly depend on the ellipsoidal shape and less so on the anisotropy of the flow.

A first analysis of the single particle spectra, elliptic flow and azimuthally sensitive HBT radii was presented. The formulas obtained from the full Buda-Lund model yield a reasonable description of these data with a reasonable choice of the model parameters, indicating, that the ellipsoidally symmetric Buda-Lund model has reasonable properties when compared to azimuthally sensitive HBT data.

Note that the present formulas were obtained in a Gaussian approximation to the proper-time distribution and to the saddle-point integration of the source function. Non-Gaussian features were reported earlier when performing an advanced saddle point integration - deviations from Gaussian HBT correlations were predicted in the longitudinal direction already in the azimuthally symmetric version, see e.g. [22]. Also, a non-Gaussian proper-time distribution would result in non-Gaussian distributions in directions coupled to the out direction, but these effects are not explored in the current manuscript.

A unique feature, which could eventually falsify the use of the single saddle point approximation and the Gaussian version of the Buda-Lund model for the description of data is the fact that there is only explicit and no implicit azimuthal dependence of the correlation radii. In such models oscillation amplitudes of R_s^2 , R_o^2 , and R_{os}^2 are the same. Precise data could resolve if this is really the case.

However, some of the conclusions like the fireball freezes out early, when $X \simeq Y$ but $\dot{X} > \dot{Y}$, seem to be robust features of the data, as these features are obtained in different models like the Buda-Lund and the blast-wave models independently.

More work has to be done to explore more quantitatively the fitting procedure, the error estimation and the confidence level tests, using the full formulas.

Acknowledgments This paper was prepared within a bilateral collaboration between Hungary and Slovakia under project Nos. SK-20/2006 (HU), SK-MAD-02906 (SK). B.T. acknowledges support by VEGA 1/4012/07 (Slovakia), MSM 6840770039, and LC 07048 (Czech Republic). M.Cs. and T.Cs. gratefully acknowledge the support of the Hungarian OTKA grants T49466 and NK 73143.

References

1. M. Riordan and W. A. Zajc, *Sci. Am.* **294N5**, 24 (2006).
2. F. Retiere and M. A. Lisa, *Phys. Rev.* **C70**, 044907 (2004) [arXiv:nucl-th/0312024].
3. E. Schnedermann, J. Sollfrank, and U. W. Heinz, *Phys. Rev. C* **48**, 2462 (1993) [arXiv:nucl-th/9307020].
4. M. Csanád, T. Csörgő, B. Lörstad, and A. Ster, *Nukleonika* **49**, S49 (2004) [arXiv:nucl-th/0402037].
5. T. Csörgő *et al.*, *Phys. Rev.* **C67**, 034904 (2003) [arXiv:hep-ph/0108067].
6. T. Csörgő, F. Grassi, Y. Hama, and T. Kodama, *Phys. Lett.* **B565**, 107 (2003) [arXiv:nucl-th/0305059].
7. Y. M. Sinyukov and I. A. Karpenko, *Acta Phys. Hung.* **A25**, 141 (2006) [arXiv:nucl-th/0506002].
8. T. Csörgő, M. I. Nagy, and M. Csanád, *Phys. Lett.* **B663**, 306 (2008) [arXiv:nucl-th/0605070].
9. S. Pratt and S. Pal, *Nucl. Phys.* **A749**, 268 (2005) [arXiv:nucl-th/0409038].
10. W. Broniowski, M. Chojnacki, W. Florkowski, and A. Kisiel, [arXiv:0801.4361].
11. N. S. Amelin *et al.*, *Phys. Rev.* **C77**, 014903 (2008) [arXiv:0711.0835].
12. T. J. Humanic, *Int. J. Mod. Phys.* **E15**, 197 (2006) [arXiv:nucl-th/0510049].
13. B. Tomášik, *AIP Conf. Proc.* **828**, 464 (2006) [arXiv:nucl-th/0509100].
14. T. Csörgő, *J. Phys. Conf. Ser.* **50**, 259 (2006) [arXiv:nucl-th/0505019].
15. M. A. Lisa, S. Pratt, R. Soltz, and U. Wiedemann, *Ann. Rev. Nucl. Part. Sci.* **55**, 357 (2005) [arXiv:nucl-ex/0505014].
16. T. Csörgő, L. P. Csernai, Y. Hama, and T. Kodama, *Heavy Ion Phys.* **A21**, 73 (2004) [arXiv:nucl-th/0306004].
17. T. Csörgő and B. Lörstad, *Phys. Rev.* **C54**, 1390 (1996) [arXiv:hep-ph/9509213].
18. M. Csanád, T. Csörgő, and B. Lörstad, *Nucl. Phys.* **A742**, 80 (2004) [arXiv:nucl-th/0310040].
19. M. Csanád, T. Csörgő, B. Lörstad, and A. Ster, *Acta Phys. Polon.* **B35**, 191 (2004) [arXiv:nucl-th/0311102].
20. T. Csörgő, M. Csanád, B. Lörstad, and A. Ster, *Acta Phys. Hung.* **A24**, 139 (2005) [arXiv:hep-ph/0406042].
21. A. Ster, T. Csörgő, and B. Lörstad, *Nucl. Phys.* **A661**, 419 (1999) [arXiv:hep-ph/9907338].
22. T. Csörgő, *Heavy Ion Phys.* **15**, 1 (2002) [arXiv:hep-ph/0001233].
23. N. M. Agababyan *et al.*, *Phys. Lett.* **B422**, 359 (1998) [arXiv:hep-ex/9711009].
24. T. Csörgő, B. Lörstad, and J. Zimányi, *Z. Phys.* **C71**, 491 (1996) [arXiv:hep-ph/9411307].
25. T. Csörgő, *Acta Phys. Polon.* **B37**, 483 (2006) [arXiv:hep-ph/0111139].
26. T. Csörgő, *Central Eur. J. Phys.* **2**, 556 (2004) [arXiv:nucl-th/9809011].
27. T. Csörgő and J. Zimányi, *Heavy Ion Phys.* **17**, 281 (2003) [arXiv:nucl-th/0206051].
28. S. V. Akkelin *et al.*, *Phys. Lett.* **B505**, 64 (2001) [arXiv:hep-ph/0012127].
29. T. Csörgő and B. Lörstad, *Nucl. Phys.* **A590**, 465c (1995) [arXiv:hep-ph/9503494].
30. M. Csanád *et al.*, [arXiv:nucl-th/0512078].
31. A. Adare *et al.*, *Phys. Rev. Lett.* **98**, 162301 (2007) [arXiv:nucl-ex/0608033].
32. S. Afanasiev *et al.*, *Phys. Rev. Lett.* **99**, 052301 (2007) [arXiv:nucl-ex/0703024].
33. B. Tomášik, *Acta Phys. Polon.* **B36**, 2087 (2005) [arXiv:nucl-th/0409074].
34. S. Pratt, *Phys. Rev.* **D33**, 1314 (1986).
35. U. W. Heinz, A. Hummel, M. A. Lisa, and U. A. Wiedemann, *Phys. Rev.* **C66**, 044903 (2002) [arXiv:nucl-th/0207003].
36. B. Tomášik and U. A. Wiedemann, in *Quark Gluon Plasma 3*, edited by R. C. Hwa and X.-N. Wang (World Scientific, Singapore, 2004), pp. 715–777. [arXiv:hep-ph/0210250]
37. S. S. Adler *et al.*, *Phys. Rev.* **C69**, 034909 (2004) [arXiv:nucl-ex/0307022].
38. J. Adams *et al.*, *Phys. Rev.* **C72**, 014904 (2005) [arXiv:nucl-ex/0409033].
39. J. Adams *et al.*, *Phys. Rev. Lett.* **93**, 012301 (2004) [arXiv:nucl-ex/0312009].